ANTIOXIDANTS & REDOX SIGNALING
Volume 27, Number 9, 2017

DOI: 10.1089/ars.2016.6848

Discoveries

ORIGINAL RESEARCH COMMUNICATION

Cardiac Light Chain Amyloidosis: The Role of Metal Ions in Oxidative Stress and Mitochondrial Damage

Luisa Diomede,[1] Margherita Romeo,[1] Paola Rognoni,[2] Marten Beeg,[1] Claudia Foray,[3] Elena Ghibaudi,[4] Giovanni Palladini,[2,5] Robert A. Cherny,[6,7] Laura Verga,[8] Gian Luca Capello,[8] Vittorio Perfetti,[9] Fabio Fiordaliso,[3] Giampaolo Merlini,[2,5] and Mario Salmona[1]

Abstract

Aims: The knowledge of the mechanism underlying the cardiac damage in immunoglobulin light chain (LC) amyloidosis (AL) is essential to develop novel therapies and improve patients' outcome. Although an active role of reactive oxygen species (ROS) in LC-induced cardiotoxicity has already been envisaged, the actual mechanisms behind their generation remain elusive. This study was aimed at further dissecting the action of ROS generated by cardiotoxic LC *in vivo* and investigating whether transition metal ions are involved in this process. In the absence of reliable vertebrate model of AL, we used the nematode *Caenorhabditis elegans*, whose pharynx is an ''ancestral heart.''

Results: LC purified from patients with severe cardiac involvement intrinsically generated high levels of ROS and when administered to *C. elegans* induced ROS production, activation of the DAF-16/forkhead transcription factor (FOXO) pathway, and expression of proteins involved in stress resistance and survival. Profound functional and structural ROS-mediated mitochondrial damage, similar to that observed in amyloid-affected hearts from AL patients, was observed. All these effects were entirely dependent on the presence of metal ions since addition of metal chelator or metal-binding 8-hydroxyquinoline compounds (chelex, PBT2, and clioquinol) permanently blocked the ROS production and prevented the cardiotoxic effects of amyloid LC.

Innovation and Conclusion: Our findings identify the key role of metal ions in driving the ROS-mediated toxic effects of LC. This is a novel conceptual advance that paves the way for new pharmacological strategies aimed at not only counteracting but also totally inhibiting the vicious cycle of redox damage. *Antioxid. Redox Signal.* 27, 567–582.

Keywords: metals, amyloid, protein misfolding, immunoglobulin light chain, *caenorhabditis elegans*, mitochondria

Introduction

ORGAN DAMAGE IN IMMUNOGLOBULIN light chain (LC) amyloidosis (AL) results from the direct toxic effects of aberrant, misfolded monoclonal LC and from the structural subversion caused by extracellular amyloid deposits in target organs (33, 34). Approximately 75% of patients manifest heart involvement at presentation. These patients experience rapid worsening of cardiac failure with a median survival of only 6 months if cytotoxic chemotherapy fails to stop plasma

[1]Department of Molecular Biochemistry and Pharmacology, IRCCS-Istituto di Ricerche Farmacologiche ''Mario Negri,'' Milan, Italy.
[2]Amyloid Research and Treatment Center, Foundation IRCCS Policlinico San Matteo, Pavia, Italy.
[3]Bio-imaging Unit, Department of Cardiovascular Research, IRCCS-Istituto di Ricerche Farmacologiche ''Mario Negri,'' Milan, Italy.
[4]Department of Chemistry, University of Turin, Turin, Italy.
[5]Department of Molecular Medicine, University of Pavia, Pavia, Italy.
[6]The Florey Institute of Neuroscience and Mental Health, The University of Melbourne, Royal Pde, Parkville, Australia.
[7]Prana Biotechnology Ltd., Parkville, Australia.
[8]Pathologic Unit and [9]Medical Oncology Unit, Foundation IRCCS Policlinico San Matteo, Pavia, Italy.

Innovation

Redox-active transition metals play a key role in driving the reactive oxygen species (ROS)-mediated toxic effects of immunoglobulin light chain (LC) in cardiac AL. Although these evidences are obtained in a simple multicellular organism, their relevance is supported by the evolutionary conservation of basic biological processes between *Caenorhabditis elegans* and humans and the similar subcellular alterations caused by cardiac LC in human heart and worms. Metal-binding 8-hydroxyquinoline compounds permanently blocked the ROS production and prevented the cardiotoxic effects of LC. This novel conceptual advance paves the way for new pharmacological strategies aimed at not only counteracting but also totally inhibiting the vicious cycle of redox damage.

cell LC production. Patients with advanced cardiac involvement (53) are frequently too fragile to tolerate chemotherapy: paradoxically, patients most in need of treatment are those who at present cannot be treated effectively.

In patients in whom chemotherapy reduces the concentration of the amyloidogenic circulating LC, cardiac dysfunction improves—despite the amyloid load remaining unaltered—suggesting that both host-related factors and intrinsic LC characteristics are required to cause organ toxicity. No clear relationship has been established between the LC germline genes and the targeting of specific organs, including the heart, and no specific features related to LC cardiotoxicity have been described yet, rendering the protein's ability to target the heart impossible to predict (39). A better understanding of the molecular and biochemical mechanisms underlying the cardiotoxicity of LC is essential to design innovative therapeutic strategies and improve patients' outcome.

The processes through which extracellular LC leads to cardiac pathology are still under investigation. Data obtained *in vitro* suggest that LC associated with cardiomyopathy has an intrinsic and specific cardiotoxic potential and involves different processes such as increased apoptosis, oxidative stress, and the activation of specific signal transduction pathways (8).

To develop novel therapeutic strategies, facilitate early diagnosis, and investigate the mechanisms of toxicity, the development of experimental models that are able to recapitulate LC cardiotoxicity remains a major and urgent need. Great efforts have been spent over the years to generate appropriate animal models that recapitulate the heart-specific toxicity of LC. Despite multiple attempts by different groups, no transgenic vertebrate animals expressing human LC have been obtained. Experiments performed on isolated mouse hearts have shown that the infusion of LC purified from patients with cardiac involvement increases end-diastolic pressure (30). Similar results were obtained in zebrafish, in which the injection of LC from patients with cardiac involvement caused a reduction in cardiac output and early mortality (35).

New hints come from studies recently performed on *Caenorhabditis elegans*, a valuable animal model for investigating the pathogenic effects of monoclonal LC *in vivo* (13). The pharynx of this nematode is an ''ancestral heart'' (31), evolutionarily related to the vertebrate heart. Its muscle cells have autonomous contractile activity, reminiscent of cardiac myocytes, and the electrical coupling between muscle cells, calcium-based action potentials, and high mitochondrial density resemble those present in mammalian heart (3, 47, 48, 56). The rhythmic contraction and relaxation of the nematode's pharyngeal muscle is responsible for the ingestion and transport of food from the mouth to the intestine. Stress-induced inhibition of feeding was suggested as an important survival mechanism that limits the intake of toxic solutes. In fact, pharyngeal pumping is inhibited by chemical stressors that induce the production of cellular stress proteins.

This nematode-based approach offers many advantages; it is more rapid, less expensive, and avoids the ethical issues involved with the use of vertebrate animals such as rodents and zebrafish. In addition, the small amount of human LC required to perform the analysis renders this assay feasible for future routine clinical analysis. All these features render *Caenorhabditis elegans* as the most feasible approach for studying the mechanisms of LC-induced toxicity *in vivo* and screening new drugs.

The propensity of cardiotoxic LC to generate reactive oxygen species (ROS) rendered these proteins recognizable

FIG. 1. Effect of metal ions on the ability of LC to generate ROS and affect pharyngeal pumping in worms. (A) H_2O_2 produced by cardiotoxic LC (H7-BJ) and myeloma (MM2-BJ) incubated 2 h with or without 5 mg/ml chelex. Mean ± SE of fluorescence intensity (FI), $n = 6$, $^{**}p < 0.01$ *vs*. cardiotoxic LC and $^{\circ\circ}p < 0.01$ *vs*. myeloma, one-way ANOVA and Bonferroni's *post hoc* test. **(B)** Worms were fed for 2 h with 100 μg/ml cardiotoxic LC (H6-BJ, H7-BJ, H7-r, H18-BJ), myeloma proteins (MM2-BJ, MM4-BJ, MM7-BJ) with or without 5 mg/ml chelex or 10 μM ethylenediaminetetraacetic acid. Control worms were incubated with 10 mM PBS, pH 7.4 (Vehicle) only (*dotted line*). The mean ± 95% CI of pumps/min was calculated (*horizontal line*). Each *dot* is the mean of pumps/min for each protein (3 independent assays, $n = 30$ worms/assay). $^{**}p < 0.01$ *vs*. Vehicle, $^{\circ\circ}p < 0.01$ *vs*. cardiotoxic LC, one-way ANOVA and Bonferroni's *post hoc* test. **(C)** H_2O_2 produced by 45 μM cardiotoxic LC and myeloma treated with chelex and incubated 2 h with 50 μM $CuCl_2$, $ZnCl_2$, or $FeCl_2$. Control samples were incubated with chelex-treated 10 mM PBS, pH 7.4. Mean ± SE of FI, $n = 12$, $^{**}p < 0.01$ *vs*. cardiotoxic LC incubated with chelex-treated PBS, pH 7.4, $^{\circ\circ}p < 0.01$ *vs*. myeloma LC + chelex-treated PBS, pH 7.4, one-way ANOVA and Bonferroni's *post hoc* test. **(D)** Worms were fed for 2 h with 100 μg/ml cardiotoxic LC (H7-BJ), myeloma (MM2-BJ) with or without 50 μM $CuCl_2$, $ZnCl_2$, or $FeCl_2$. Control worms were incubated with 10 mM PBS, pH 7.4 (Vehicle) only or 50 μM $CuCl_2$, $ZnCl_2$, and $FeCl_2$. Pumping rate as mean pumps/min ± SE ($n = 20$ worms/assay, three assays). $^{**}p < 0.01$ *versus* vehicle, one-way ANOVA and Bonferroni's *post hoc* test.$^{\circ\circ}p < 0.0001$ *versus* cardiotoxic LC, two-way ANOVA and Bonferroni's *post hoc* test. **(E)** H_2O_2 produced by cardiotoxic LC (H7-BJ) and myeloma (MM2-BJ) previously treated for 3 h at 20°C with iodoacetamide and then incubated 2 h with 50 μM $CuCl_2$. Mean ± SE of FI, $n = 9$, $^{**}p < 0.01$ *versus* cardiotoxic LC not treated with iodoacetamide and $^{\circ\circ}p < 0.01$ *vs* cardiotoxic LC treated with iodoacetamide, one-way ANOVA and Bonferroni's *post hoc* test. ANOVA, analysis of variance; BJ, Bence Jones; LC, immunoglobulin light chain; PBS, phosphate-buffered saline; ROS, reactive oxygen species.

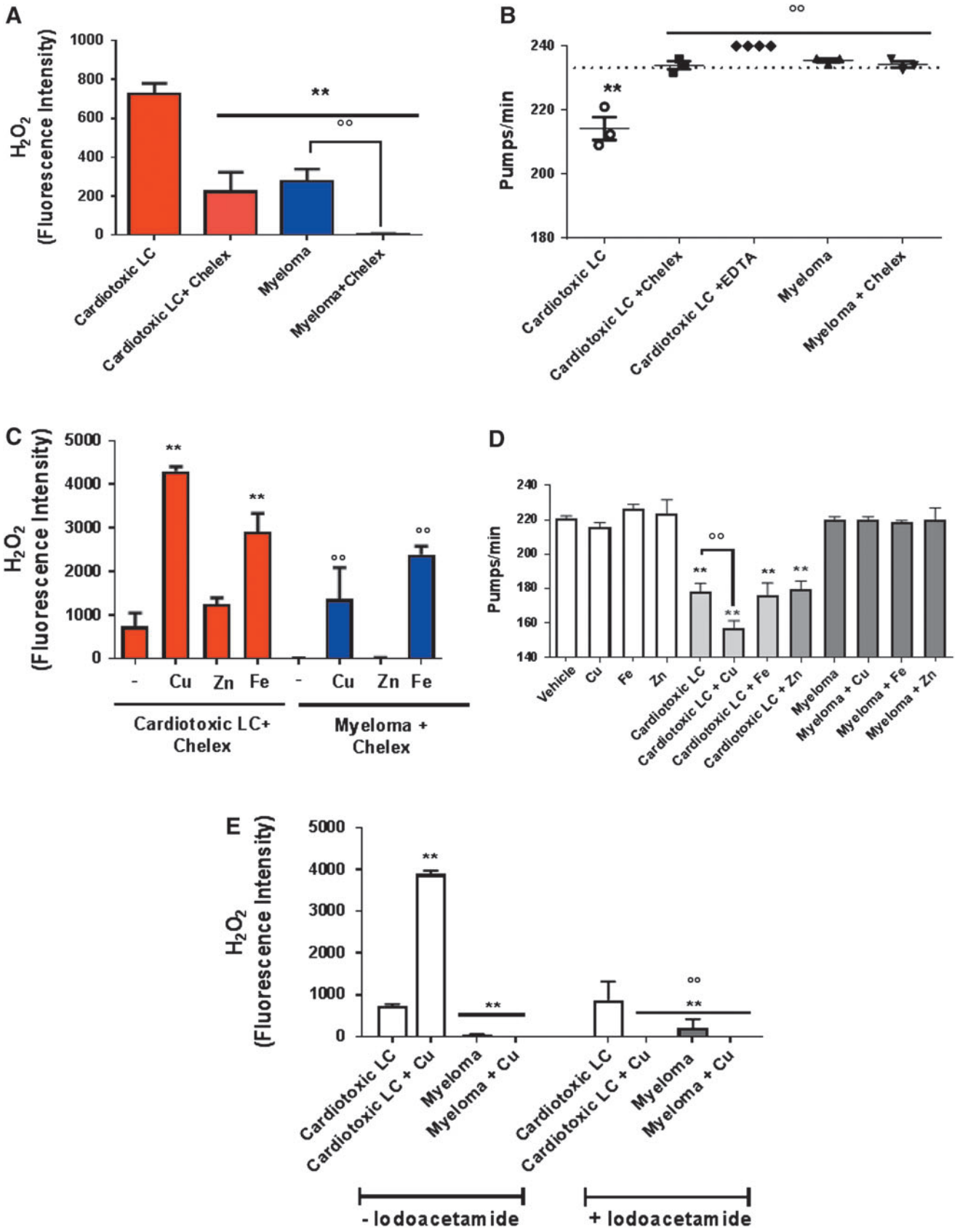
A
H_2O_2 (Fluorescence Intensity)
1000
800
600
400
200
0
**
°°
Cardiotoxic LC
Cardiotoxic LC+ Chelex
Myeloma
Myeloma+Chelex
B
Pumps/min
240
220
200
180
°°
**
Cardiotoxic LC
Cardiotoxic LC +Chelex
Cardiotoxic LC +EDTA
Myeloma
Myeloma + Chelex
C
H_2O_2 (Fluorescence Intensity)
5000
4000
3000
2000
1000
0
**
**
°°
°°
-
Cu
Zn
Fe
-
Cu
Zn
Fe
Cardiotoxic LC+ Chelex
Myeloma + Chelex
D
Pumps/min
240
220
200
180
160
140
°°
**
**
**
**
Vehicle
Cu
Fe
Zn
Cardiotoxic LC
Cardiotoxic LC + Cu
Cardiotoxic LC + Fe
Cardiotoxic LC + Zn
Myeloma
Myeloma + Cu
Myeloma + Fe
Myeloma + Zn
E
H_2O_2 (Fluorescence Intensity)
5000
4000
3000
2000
1000
0
**
**
°°
**
Cardiotoxic LC
Cardiotoxic LC + Cu
Myeloma
Myeloma + Cu
Cardiotoxic LC
Cardiotoxic LC + Cu
Myeloma
Myeloma + Cu
- Iodoacetamide
+ Iodoacetamide

as ''stressors'' by worms (13). Cardiotoxic LC also enhanced ROS production by mitochondria, causing permanent pharyngeal dysfunction and reducing life span. Importantly, administration of antioxidant drugs *N*-acetyl-cysteine (NAC) and tetracycline hydrochloride (TETRA), prevented these effects (13), indicating that ROS generated by amyloidogenic cardiotoxic LC actively contribute to their detrimental activity *in vivo.* Strategies aimed at halting the vicious cycle of oxidative stress might provide innovative and potentially less toxic options, specifically aimed at not only counteracting but totally inhibiting the vicious cycle of redox damage.

We here report that ROS produced by cardiotoxic LC act as signaling molecules in *C. elegans*, activating the Forkhead transcription factor (FOXO)/DAF-16 pathway (37) and controlling genes involved in stress resistance and survival. LC also caused a remarkable ultrastructural alteration in the pharynx of worms and mitochondrial damage similar to that observed in amyloid-affected hearts from AL patients.

Metal ions play a key role in driving all these effects, suggesting metal-binding agents as a compelling pharmacological strategy for AL.

The metal chelating resin chelex and two transition metal-binding compounds, members of the 8-hydroxyquinoline chemical class, were considered: clioquinol (5-chloro-7-iodo-quinolin-8-ol, CQ) and PBT2 (44). CQ is a legacy compound while PBT2 is a novel noniodinated analog that has been shown to assist in restoration of metal homeostasis (44). All compounds reduced the ability of cardiotoxic LC to generate ROS and counteracted their related functional and structural damage on the worm's pharynx. Notably, the administration of pharmacologic low doses of PBT2 in combination with tetracyclines, which reduced early deaths in patients with cardiac AL when added to standard chemotherapy (52), resulted in a synergistic beneficial effect, highlighting the potential application of this pharmacological strategy for cardiac AL patients.

Results

Metal ions drive ROS generation and pharyngeal damage

The pharyngeal *C. elegans* impairment caused by the administration of cardiotoxic LC, at 100 μg/ml, a concentration representative of serum-free LC in AL patients, was related to the capacity to generate ROS, particularly within mitochondria (13). The role of transition metal ions in regulating the ability of LC to produce ROS was investigated here. To this end, monoclonal LC were purified from three patients with cardiac AL and from three negative control patients with multiple myeloma (MM) (Supplementary Table S1; Supplementary Data are available online at www.liebertpub.com/ars).

Cardiotoxic LC, already reported to produce a greater amount of oxygen radicals, particularly $^{\bullet}OH$ radical species, compared to myeloma (13), intrinsically generated significantly higher levels of H_2O_2 (725 ± 55.8 *vs.* 278 ± 61.9 fluorescence intensity [FI] value for cardiotoxic LC and myeloma, respectively, $p < 0.01$, Fig. 1A). ROS generation was significantly attenuated when metal ions were chelated eluting protein on chelex, a metal-chelating resin (Fig. 1A). In particular, chelex reduced the H_2O_2 generation by cardiotoxic LC of 69% (725 ± 55.8 FI in cardiotoxic LC and 222 ± 101 FI in cardiotoxic LC + chelex) and fully abolished its production by myeloma (278 ± 61.9 FI in myeloma and 4.17 ± 4.09 in myeloma + chelex) (Fig. 1A).

The residual ROS produced by cardiotoxic LC after chelex exposure might be due to partial removal of metals, since chelex is notoriously unreliable at removing trace metals. Metal chelation did not affect the secondary structure content and thermostability of LC (Supplementary Fig. S1).

The specific involvement of H_2O_2 on the *C. elegans* impairment caused by the administration of cardiotoxic LC was investigated using catalase. To this end, cardiotoxic and myeloma proteins were incubated with 100 U/ml of catalase for 15 min before administration to worms. Catalase, at this concentration, was effective to completely abolish the pharyngeal dysfunction induced by 1 m*M* H_2O_2 and counteracted the toxicity caused by cardiotoxic LC but not myeloma feeding (Supplementary Fig. S2).

When cardiotoxic proteins purified from patients with severe amyloid cardiomyopathy were treated with chelex and administered to worms in metal-free water, their ability to cause pharyngeal dysfunction was abolished, whereas no change was observed when myeloma proteins were eluted on chelex (Fig. 1B). Similar results were obtained when LC were coadministered in metal-free water with the generic metal chelator ethylenediaminetetraacetic acid (EDTA) (17) (Fig. 1B).

The addition of copper and iron, but not zinc, to cardiotoxic and myeloma proteins treated with chelex restored their native ability to produce H_2O_2 (Fig. 1C). When copper was added to the protein solution, the pharyngeal dysfunction induced by cardiotoxic LC worsened, whereas iron and zinc did not exert any additional effect (Fig. 1D). A similar effect was observed when copper was administered together with chelex-treated cardiotoxic protein (Supplementary Fig. S3). The pumping rate of *C. elegans*-fed myeloma protein was not affected by either copper or iron and zinc (Fig. 1D). These results indicate that both iron and copper can drive the generation of H_2O_2 by cardiotoxic and myeloma proteins in cell-free conditions, but only copper exerts an active role in the pharyngeal toxicity.

Copper has already been reported to be able to bind to amyloidogenic LC (12). To search for a direct interaction of copper with LC, near and far-UV circular dichroism (CD) spectra were recorded, as well as tryptophan fluorescence measurements. No significant modifications indicative of direct binding of copper to cardiotoxic and myeloma proteins were observed (data not shown), suggesting that the interaction of this metal with LC is transient, local, and relatively weak.

However, the increase in H_2O_2 production by cardiotoxic LC in the presence of copper proves that the metal was reduced from Cu^{2+} to Cu^{+} by the protein, suggesting that proteins must possess reducing species (most commonly thiols such as cysteine) to donate electrons (38). The preincubation of cardiotoxic LC with iodoacetamide—which links covalently with the thiols and thus prevents them from being a source of electrons (54)—cleared the copper-induced increased production of H_2O_2 (Fig. 1E), demonstrating that an interaction between protein and copper is necessary for radical production.

Electron paramagnetic resonance (EPR) measurements performed on cardiotoxic LC show that copper enhances the radical production, although a linear dependence between copper concentration and amount of radical could not be

established. This is likely due to the fact that the redox cycling process is catalytic; hence, it does not follow linear kinetics (Supplementary Fig. S4).

Furthermore, we observed that the feeding of *C. elegans* with cardiotoxic LC, but not myeloma, resulted in a specific increase in endogenous copper levels (Supplementary Fig. S5A), whereas iron and zinc ion levels were not significantly altered (Supplementary Fig. S5B).

Metal-binding compounds counteracted the cardiotoxic LC-induced functional and structural damage on the worm's pharynx

The effect of CQ and PBT2 was considered. Their effect in counteracting the pharyngeal dysfunction caused by cardiotoxic LC was dose dependent (Fig. 2A), PBT2 being significantly more effective than CQ, with an IC_{50} ~7000-fold lower (IC_{50}: 1.08 ± 1.1 n*M* and 7.5 ± 1.0 μ*M* for PBT2 and CQ, respectively; $p < 0.01$, Student's t test). We settled on an optimal concentration of 25 μ*M* for CQ and 2 n*M* for PBT2, dose levels that caused a 98% redution of H_2O_2 production (Fig. 2B) and completely abolished the pharyngeal impairment caused by all cardiotoxic LC under investigation (Fig. 2C). At these concentrations CQ and PBT2 did not affect the secondary structure content and thermostability of LC (Supplementary Fig. S1).

Noteworthy, CQ and PBT2 exerted similar effects on both natural BJ and recombinant LC from the same cardiac amyloid patient (Supplementary Table S2), indicating that the particular ability of amyloid cardiac LC to interact with metal ions was not an artifact of the protein purification procedure. CQ and, to a lesser extent, PBT2, counteracted the cardiotoxic LC-induced

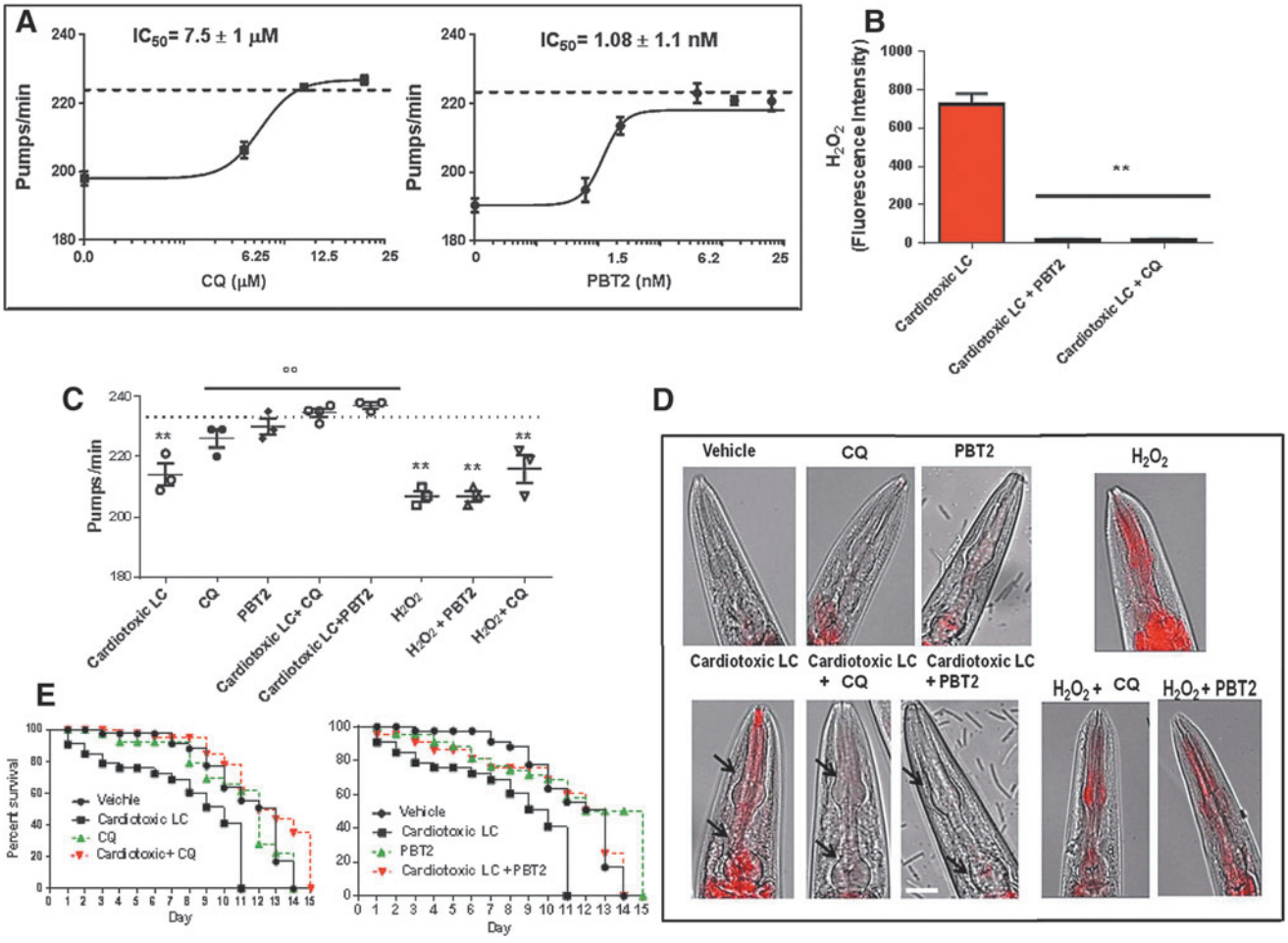

FIG. 2. Effect of metal-binding compounds CQ and PBT2 on LC-induced H_2O_2 production and oxidative damage. **(A)** Dose–response effect of CQ and PBT2 on LC-induced pharyngeal dysfunction. Worms were fed for 2 h with 100 μg/ml cardiotoxic LC in the absence or presence of 0–25 μ*M* CQ or 0–25 n*M* PBT2. Control worms received vehicle alone (*dotted line*). Each value is the mean ± SE, $n = 30$. IC_{50} ± SD are reported, $p < 0.01$, Student's *t*-test. **(B)** H_2O_2 produced by cardiotoxic LC (H7-BJ) incubated 2 h with or without 2 n*M* PBT2 or 25 μ*M* CQ. Mean ± SE of FI, $n = 6$, $^{**}p < 0.01$ *versus* cardiotoxic LC, one-way ANOVA and Bonferroni's *post hoc* test. **(C, D)** Worms were fed for 2 h with 100 μg/ml cardiotoxic LC (H6-BJ, H7-BJ, H7-r, H18-BJ) with or without 25 μ*M* CQ or 2 n*M* PBT2. H_2O_2 (1 m*M*) was administered for 30 min with or without the drugs. Control worms received vehicle alone (*dotted line*). **(C)** The mean ± 95% CI of pumps/min was calculated (*horizontal line*). Each *dot* is the mean of pumps/min for each protein (3 independent assays, $n = 30$ worms/assay). $^{**}p < 0.01$ *versus* Vehicle, $^{\circ\circ}p < 0.01$ *versus* cardiotoxic LC, one-way ANOVA and Bonferroni's *post hoc* test. **(D)** Images obtained from the overlay of a contrast phase and MitoSOX fluorescence (*arrows*). Scale bar 50 μm. **(E)** Kaplan–Meier survival curves, $n = 30$ worms/group, three independent experiments. CQ, 5-chloro-7-iodo-quinolin-8-ol.

elevation of copper levels in worms, without affecting the levels of iron or zinc (Supplementary Fig. S5). CQ binds iron with moderate affinity, but PBT2 is a poor ligand for iron (43). Because both compounds bind copper with similar affinity, this element is the most likely redox-active binding partner involved in cardiotoxic LC-induced dysfunction.

Neither compound counteracted H_2O_2-induced pharyngeal toxicity (Fig. 2C), indicating that their protective effect against cardiotoxic LC is not related to a general antioxidant activity. This conclusion was further supported by the fact that CQ and PBT2 protected nematodes against the increase in mitochondrial ROS generation caused by cardiotoxic LC but not H_2O_2 (Fig. 2D). Drugs alone did not modify the pumping rate (Fig. 2C) nor the increase of pharyngeal mitochondrial oxygen burden (Fig. 2D).

As already reported (13), the exposure of *C. elegans* to cardiotoxic LC significantly reduced their life span (median survival: 13 and 9 days for vehicle- and cardiotoxic LC-fed worms, respectively, $p = 0.0001$, Log-rank test) (Fig. 2E). A single dose of 25 μM CQ and administration of 2 n*M*/day PBT2 significantly prolonged the survival of cardiotoxic LC-treated worms, restoring their natural life span (median survival: 14 days for cardiotoxic LC + CQ-treated worms ($p = 0.036$ *vs.* cardiotoxic LC) and 13 days for cardiotoxic LC +2 n*M*/day PBT2 ($p = 0.025$ *vs.* cardiotoxic LC)) (Fig. 2E).

We investigated whether ROS produced by cardiotoxic LC caused alterations in pharyngeal subcellular compartments, particularly mitochondria, which play a vital role in providing energy for contractile activity. Transmission electron microscopy (TEM) analyses showed that the pharyngeal muscles of worms fed cardiotoxic LC, but not myeloma protein, resulted in profound alteration of the pharyngeal ultrastructure and caused mitochondrial damage compared with vehicle-treated nematodes (Fig. 3A–C). These morphological alterations were accompanied by impaired mitochondrial function, as demonstrated by the decreased membrane potential, which was determined using the fluorescent probe tetramethylrhodamine, methyl ester (TMRM) (Supplementary Fig. S6).

Since similar features were observed when worms were fed all the cardiac amyloid LC considered in the study, which derived from unrelated germline gene, this indicated that the observed functional and structural effects were strictly dependent on features that are intrinsic to cardiac LC, with no restriction to a particular germline gene or set of genes.

The subcellular alterations observed in worms were comparable to damage caused by cardiac LC in human heart tissue as proved by endomyocardial biopsies from AL patients with advanced cardiac dysfunction (Supplementary Table S3) analyzed by TEM. Similar to worms exposed to cardiac LC, most human mitochondria showed dramatic structural derangement (Fig. 4A–C and Supplementary Fig. S7): their size was enlarged and also the cristae formed by the internal membrane were almost totally lost. In contrast, endomyocardial biopsies from subjects who had undergone heart transplantation for primary dilated cardiomyopathy (used as controls for disease and severity of heart dysfunction) showed fully preserved

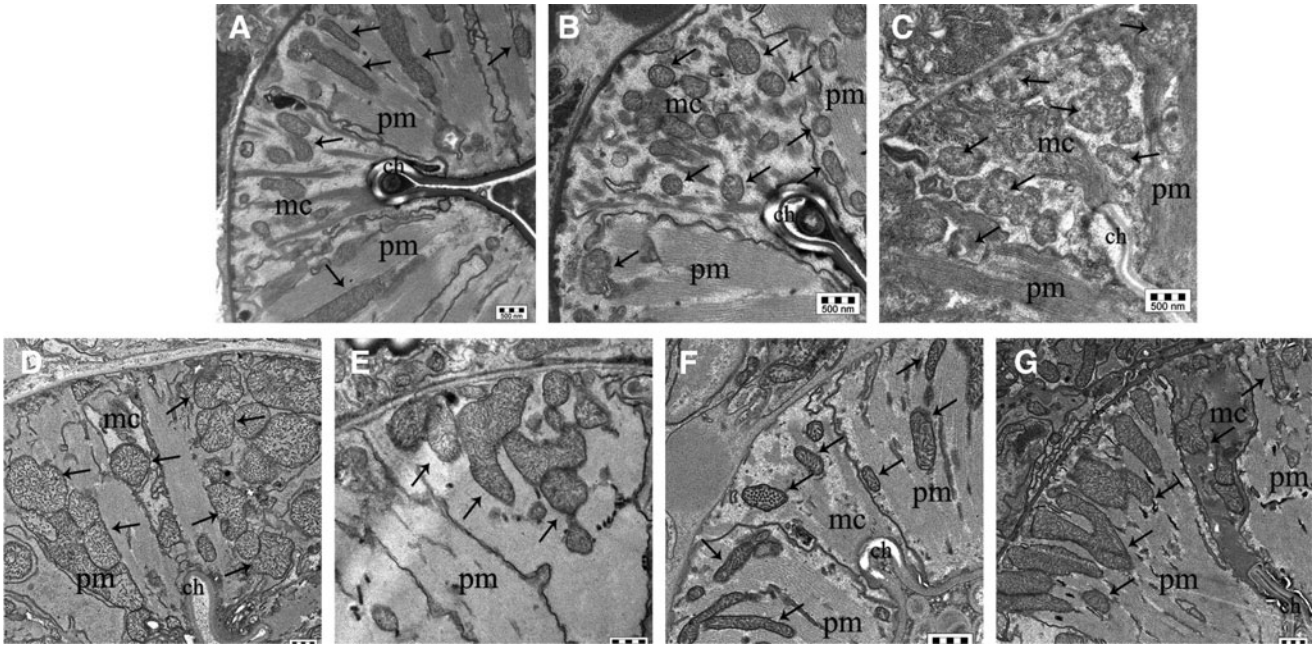

FIG. 3. ROS-induced cardiotoxic LC severely disrupt *Caenorhabditis elegans* pharyngeal ultrastructure. (A–G) Representative images of worm's pharynx obtained from the ultrastructural analysis by TEM in *C. elegans* fed for 2 h with **(A)** Vehicle, **(B)** myeloma protein (MM2-BJ), **(C)** cardiotoxic LC (H7-BJ) alone, or with **(D)** 25 μM CQ, **(E)** 2 n*M* PBT2, **(F)** 50 μM TETRA, or **(G)** 5 m*M* NAC. Images showed two *pharyngeal muscles* (pm) separated by a *marginal cell* (mc), placed at the corner of the *pharyngeal channel* (ch). Mitochondria are indicated by *arrows*. Scale bar, 500 nm. Pharyngeal muscles of worms fed cardiotoxic LC resulted in damage to mitochondria, which exhibited a clustering pattern, irregular shape, swelling, and massive disruption of the internal components (*i.e.*, cristae). Marginal cells, which contain many mitochondria due to their active role in contractile motor function, were seriously compromised and myofilaments connected to the marginal cells, which were perfectly aligned in vehicle-fed worms, were deranged. NAC, *N*-acetyl-cysteine; TEM, transmission electron microscopy; TETRA, tetracycline hydrochloride.

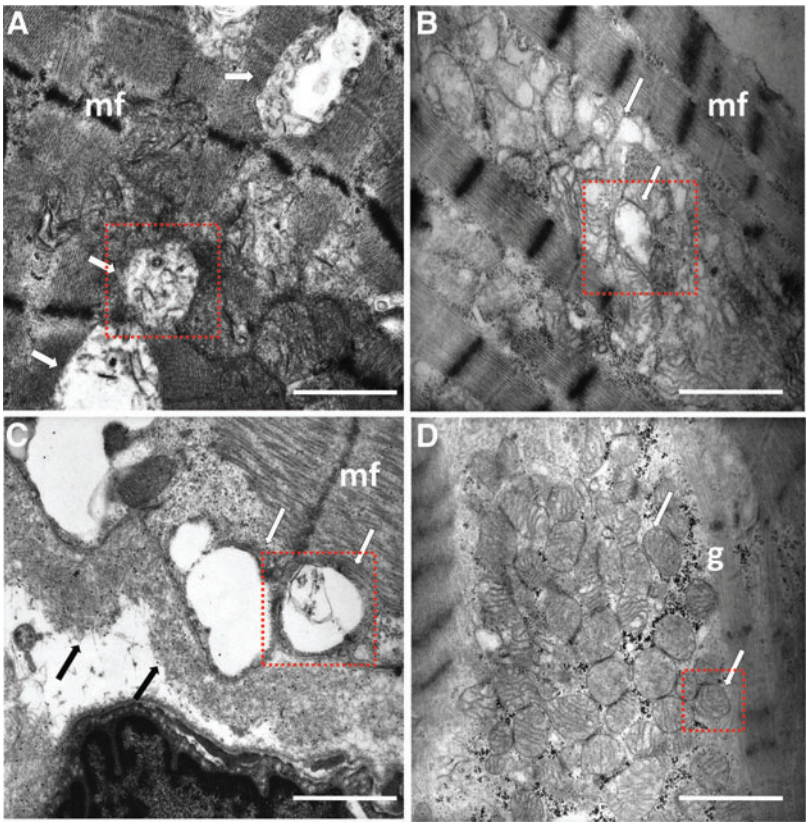

FIG. 4. Mitochondrial damage in heart muscle tissue of cardiac AL patients. Ultrastructural details from representative TEM images of endomyocardial biopsies from **(A–C)** severe cardiac amyloid AL patients and **(D)** a patient affected by dilatative cardiomyopathy. Although *myocardial fibers* (mf) are relatively well preserved in AL patients, most mitochondria (*white arrows*) show remarkable alterations with enlarged size and disruption **(A)** or total loss of cristae **(B, C)**. LC were identified by postembedding immunogold staining with 15 nm gold-conjugated protein A (*black arrows*) in the interstitium and along the basement membrane of a myocardial fiber. **(D)** The myocardium of a patient with nonamyloid cardiomyopathy shows well-preserved mitochondria (*white arrows*) and glycogen deposits (g). To better highlight the differences in damage, individual mitochondria in the *red insets* are shown in Supplementary Fig. S7. Uranyl acetate, lead citrate. Scale bar, 1 μm.

mitochondria, both in size and morphology, and only scattered mitochondria with minor alterations (Fig. 4D).

These results, resembling those reported by Guan *et al.*(21), lend support to the validity of the nematode model and reinforce the rationale of its use for designing and testing new therapeutic approaches.

When administered to *C. elegans*, PBT2 and CQ were capable of protecting the pharyngeal cells from mitochondrial-induced damage (Fig. 3D–G). A similar effect was observed with 50 μM TETRA, an antibiotic that has also antioxidant and metal ion chelator activity (10, 49), and 5 mM NAC, a prototypic antioxidant compound, which were both capable of neutralizing the ROS generation (13) and pumping dysfunction caused by cardiotoxic LC (Supplementary Fig. S8). These findings indicated that ROS are responsible for the specific ability of cardiotoxic LC to damage subcellular pharyngeal structures, particularly mitochondria.

Metal ions drive the ability of cardiotoxic LC to regulate genes involved in oxidative stress resistance

In *C. elegans*, an increase in ROS levels can result in the activation of the insulin/insulin growth factor-1 (I/IGF-1) signaling pathway (4, 23), driving the translocation of the FOXO/DAF-16, which actively controls diverse target genes involved in oxidative stress resistance and survival (37). We observed that ROS generated by cardiotoxic LC act as signaling molecules modulating the FOXO signaling pathway. Under basal conditions, DAF-16 was mainly localized in the cytosol of transgenic TJ356 *C. elegans* nematodes expressing green fluorescent protein (GFP) under control of *daf-16* promoter (23) (Fig. 5A).

The administration of cardiotoxic LC caused a significant increase of the nuclear translocation of DAF-16, detectable as the appearance of condensed green foci in the bodies of the worms (Fig. 5B). The nuclear localization was confirmed by the colocalization of the blue fluorescent dye specific for nuclei (Supplementary Fig. S9). A similar effect was observed when nematodes were fed H_2O_2 as a positive control (Supplementary Fig. S10A). CQ and PBT2 counteracted the activation of DAF-16 induced by the cardiotoxic LC (Fig. 5C, D). A similar effect was observed with 50 μM TETRA, but not with 5 mM NAC (Fig. 5C, D).

The adaptive responses of the antioxidant defense system were then determined by evaluating the expression of two genes transcriptionally targetted by DAF-16. In particular,

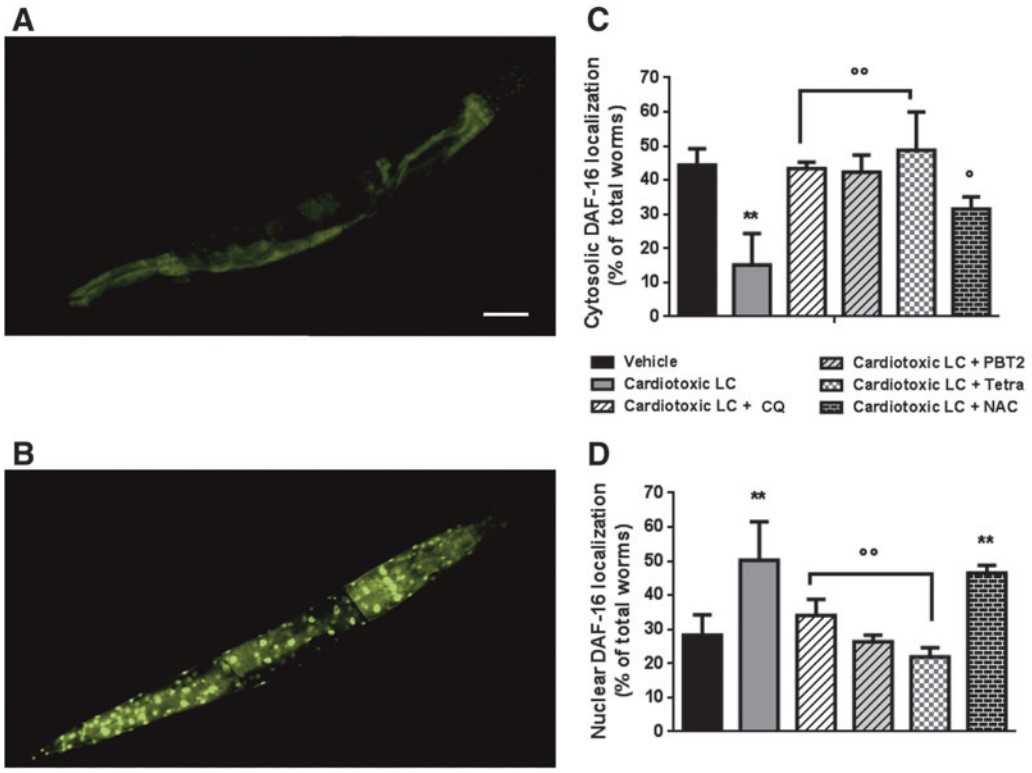

FIG. 5. Metal ions drive the ability of cardiotoxic LC to promote DAF-16 translocation from cytoplasm to nucleus in TJ356 transgenic worms. (A, B) Image of DAF-16::GFP expression in **(A)** control vehicle-fed and **(B)** cardiotoxic LC-fed worms (100 μg/ml H7-BJ for 2 h). **(C, D)** The subcellular distribution of DAF-16 expression in worms fed 2 h: vehicle, 100 μg/ml cardiotoxic LC with or without 25 μM CQ, 2 nM PBT2, 50 μM TETRA, or 5 mM NAC. According to DAF-16 localization, worms were divided into two phenotypes, including ''cytosolic'' and ''nuclear.'' The percentage of DAF-16 localization in respect to vehicle-fed worms was calculated based on three experiments, $n = 100$. Mean ± SE. ** $p < 0.01$ *versus* vehicle, °$p < 0.05$ and °°$p < 0.01$ *versus* cardiotoxic LC, one-way ANOVA and Bonferroni's *post hoc* test. GFP, green fluorescent protein.

activation of the expression of small heat shock protein (HSP)-16.2, which can act as an ROS sensor and also affects the life span of worms (23), and the activity of the antioxidant enzyme manganese superoxide dismutase (SOD)-3 were determined using transgenic CL2070 (23) and CF1553 (2) worms, expressing GFP control of *hsp-16.2* or *sod-3* promoter, respectively. It is in fact known that among the five SODs encoded and expressed by *C. elegans*, SOD-2 and SOD-3 are MnSODs localized in the mitochondrial matrix (4, 25, 36). SOD-2 contributes to the SOD activity during normal development, whereas *sod-3* is specifically upregulated by *daf-16* gene in response to ROS-induced stress.

Cardiotoxic LC, but not myeloma, caused a significant increase in HSP-16.2 (Fig. 6A, B) as well as SOD-3 expression (Fig. 6C, D) in the pharynx of nematodes, similarly to that observed with H_2O_2 (Supplementary Fig. S10B). In contrast, exposure to CQ and PBT2 significantly reduced the LC-induced HSP-16.2 and SOD-3 protein expression, as indicated by the absence of GFP signal in the pharynx of CL2070 and CF1553 worms, respectively (Fig. 6).

Overall, these results indicated that cardiotoxic LC, by means of metal ion-mediated ROS production and consequent FOXO/DAF-16 pathway activation, stimulates genes involved in the control of the oxidative stress response and life span, and that LC coincubation with metal-binding compounds, such as CQ and PBT2, abolished the worm stress response.

PBT2 and tetracycline exert a synergic effect

Based on the preclinical observations obtained in *C. elegans* on the protective effect of tetracyclines (13), a clinical study has been recently designed aimed at evaluating the cardioprotective effect of doxycycline on the heart of AL patients. Preliminary data indicated that when doxycycline was orally administered at 100 mg twice daily (corresponding to about 100 μM/day) in addition to standard chemotherapy, the early deaths in patients with cardiac AL were reduced (52).

We here analyzed whether the administration of a metal-binding agent can improve the effect of tetracyclines in *C. elegans*. In anticipation of clinical application, we set out the concentration of TETRA at 20 μM, a dose lower than that used in clinic. To reflect circumstances most likely encountered in the clinic, we designed experiments in which drugs were administered to worms for 30 min when the pharynx was already damaged by cardiotoxic LC. As expected, in these experimental conditions 20 μM TETRA was ineffective, whereas 2 nM PBT2, but not 25 μM CQ, was capable of restoring the pharyngeal dysfunction caused by cardiotoxic LC (Fig. 7A).

To determine the lowest effective dose of PBT2 able to improve the effect of TETRA, this metal-binding compound was administered at 2 or 0.5 nM concentrations. Interestingly, PBT2, at the ineffective concentration of 0.5 nM, when

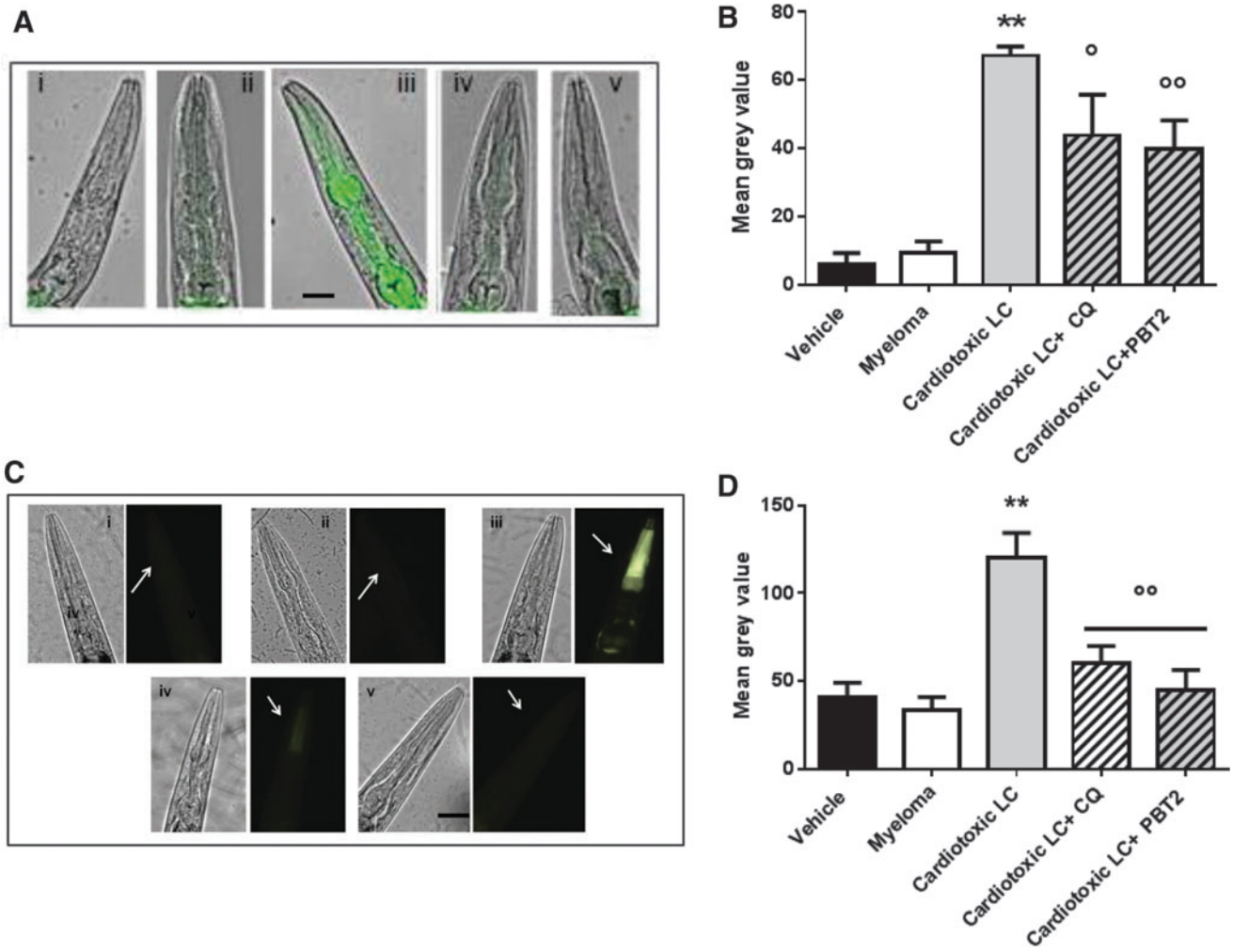

FIG. 6. Metal ions drive the ability of cardiotoxic LC to induce the pharyngeal expression of HSP-16.2 and SOD-3. **(A–D)** Transgenic worms were fed for 2 h with Vehicle **(i**, 10 m*M* PBS, pH 7.4), 100 μg/ml myeloma **(ii**, MM2-BJ), 100 μg/ml cardiotoxic LC **(iii**, H7-BJ), cardiotoxic LC +25 μ*M* CQ **(iv)** or 2 n*M* PBT2 **(v**, cardiotoxic LC + PBT2**)**. **(A)** Images of HSP-16.2 expression as overlays of GFP fluorescence and light microscopy in CL2070 transgenic worms. Scale bar, 50 μm. **(C)** Images of SOD-3 expression as GFP fluorescence (*arrows*) in CF1553 transgenic worms. Scale bar, 50 μm. Quantified GFP intensity in **(B)** CL2070 and **(D)** CF1553 worms in response to treatments. FI in each group was calculated as mean *gray* value ± SE based on three experiments, $n = 25$. $^{**}p < 0.01$ *versus* Vehicle, $^{\circ}p < 0.05$ and $^{\circ\circ}p < 0.01$ *versus* cardiotoxic LC, one-way ANOVA and Bonferroni's *post hoc* test. HSP, heat shock protein; SOD, superoxide dismutase; FI, fluorescence intensity.

combined with TETRA, exerted a synergistic and beneficial effect (Fig. 7B). Although this treatment did not totally reverse the pharyngeal dysfunction to normal levels, these results suggest that the combined administration of low doses of this metal-binding compound and TETRA may represent an innovative pharmacological approach to break the vicious cycle of oxidative stress and heart damage induced by cardiotoxic LC.

Discussion

The 25% of patients with AL diagnosed with end-stage cardiac damage represent an unmet need, since no available therapy can improve their prognosis (34, 53). Innovative approaches are needed to counteract the rapidly progressing cardiac failure sustained by the direct cardiotoxicity of amyloid LC.

We performed this study to gain insights into the mechanisms by which LC can damage the hearts of AL patients exploiting the robust *C. elegans* model. The results obtained indicate that ROS both result from and promote pharyngeal oxidative damage caused by cardiotoxic LC (Fig. 8). This effect was not related to the germline gene, which is different for each LC considered, nor to the method applied to obtain the proteins, but was strictly related to the specific ability of cardiotoxic LC to interact with metal ions and produce ROS.

Metal ions, particularly copper, have previously been shown to modulate LC polymerization (12) and interact with different amyloidogenic proteins, such as β-amyloid, prions, and α-synuclein (24, 41), promoting misfolding and generating toxic oligomeric assemblies (32). We have demonstrated here that the presence of redox-active transition metals, particularly copper, is required to drive ROS

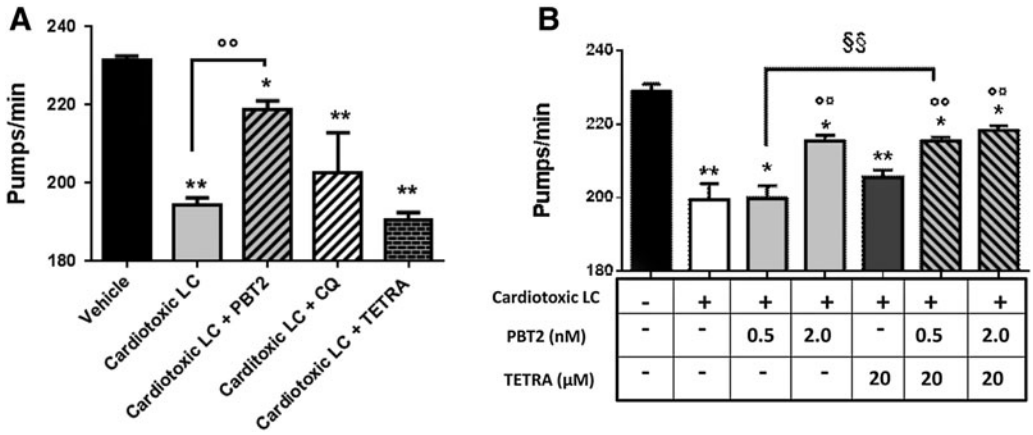

FIG. 7. Synergistic beneficial effect of PBT2 and TETRA. (A, B) Pharyngeal performance of worms fed 100 μg/ml cardiotoxic LC (H7-BJ) for 2 h and then treated for 30 min with **(A)** 25 μM CQ, 20 μM TETRA, or 2 nM PBT2 or with **(B)** 0.5–2 nM PBT2 alone or together with 20 μM TETRA. Control worms fed vehicle alone. $^{**}p<0.001$, $^{*}p<0.005$ *versus* vehicle, $^{\circ\circ}p<0.001$ *versus* cardiotoxic LC, one-way ANOVA and Bonferroni's *post hoc* test. $^{\S\S}p<0.01$ significant interaction *versus* worms fed cardiotoxic LC +0.5 nM PBT2, two-way ANOVA and Bonferroni's *post hoc* test.

production by cardiotoxic LC resulting in injurious oxidative stress to *C. elegans* pharyngeal cells.

The molecular and biochemical reasons underlying the peculiar role of copper in driving the cardiotoxic LC detrimental effects remain to be elucidated. Different activities of iron and copper in catalyzing thiol oxidation (38) and the high pharyngeal concentration of iron required to cause peroxide sensitivity and oxidative damage, which is in the millimolar range (compared to the micromolar range of copper) (50), as well as the expression of specific copper protein chaperones

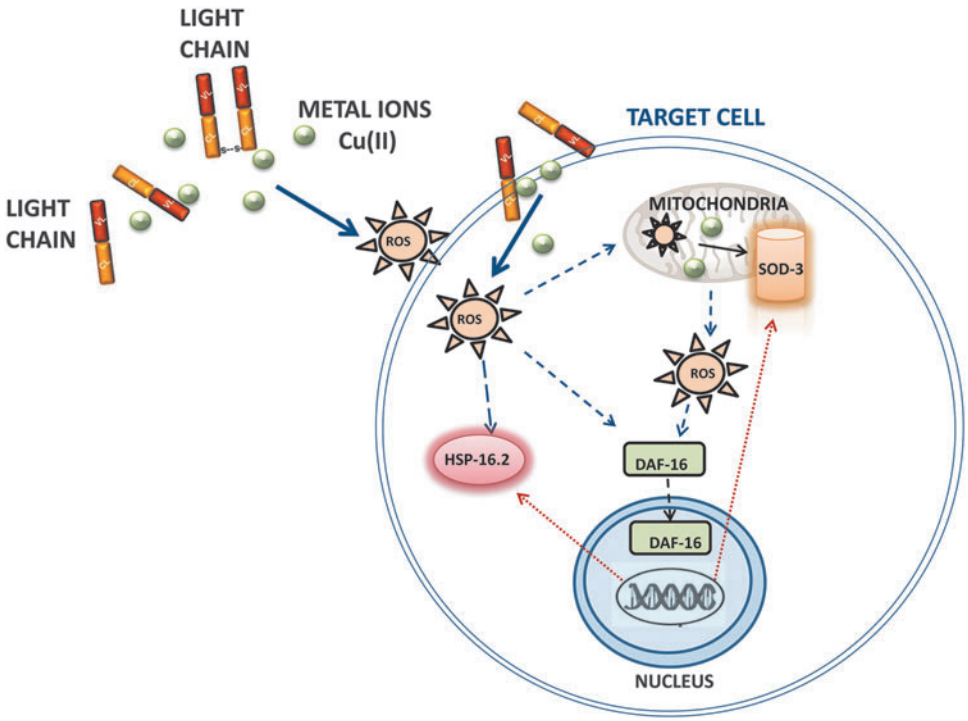

FIG. 8. Proposed model for metal ion involvement in the mechanism underlying the LC-induced toxicity. Based on our current knowledge, redox-active transition metals, particularly copper, drive the ability of cardiotoxic LC to produce ROS *in vivo*. The excessive production of ROS can directly target the pharyngeal cells, damaging the organelle functions and the ultrastructure, particularly at the mitochondrial level. ROS can be also produced as a result of the mitochondrial dysfunction requiring copper and iron for the activation of the enzymes involved in the oxidative phosphorylation pathway. Intracellular signaling events aimed at limiting and repairing the stress-induced damage are activated. Mitochondria reacts to ROS by inducing the expression of the scavenger protein SOD-3. In addition, the chaperone HSP-16.2, an αB-crystallin-related protein, is activated as well as the nuclear translocation of the FOXO/DAF-16 transcription factor. This last one can trigger a secondary ROS-induced cellular response by inducing the transcription of stress-responsive genes, including *hsp-16.2* and *sod-3*, and controlling longevity. FOXO, forkhead transcription factors.

in the pharynx (51), may be the source of the different effects exerted by the two metals. The active role of copper as the most likely redox-active binding partner is also reinforced by the fact that CQ and PBT2 bind copper with similar affinity but bind iron with moderate or low affinity, respectively (43).

ROS generated by cardiotoxic LC, in addition to causing a behavioral response in *C. elegans* that inhibited feeding (6), accumulate in the pharynx (13). Metal-mediated ROS generation also occurs within the pharyngeal cells damaging organelle functions and the ultrastructure, particularly at the mitochondrial level, resulting in disruption of their integrity. These cellular responses can trigger the permanent cellular impairment and death observed in the pharynx of worms fed cardiotoxic LC (13).

Mitochondria are naturally a rich source of ROS, usually scavenged by SOD and catalases. In the pharynx of worms fed cardiotoxic LC in response to the oxidative stress, we observed an activation of SOD-3, a protein mainly expressed in the mitochondria of pharyngeal cells (20, 25). Much of the ROS produced by mitochondria are generated by copper and iron in the active sites of the enzymes of the oxidative phosphorylation pathway. When mitochondrial membrane integrity is disrupted, the oxidative phosphorylation pathway becomes inefficient leading to extensive ROS generation, which could overwhelm the cell under conditions when it is already stressed by the toxic LC.

Data obtained by our group from human cardiac cells show that cardiotoxic LC colocalizes with mitochondria and spatially associates with selected interactors that are involved in modulating mitochondrial morphology and function and in ATP production by fatty acid β-oxidation pathway (29). Mitochondria of human cardiac cells exposed to cardiotoxic LC display ultrastructural changes, supporting the concept of mitochondrial involvement (29). Furthermore, mitochondrial damage was detected in the explanted heart from AL patients with severe cardiac involvement undergoing heart transplantation, supporting the clinical relevance of the experimental observations obtained in the *C. elegans* model. The observed disruptive effect of LC may be crucial for mitochondria-rich tissues, such as rhythmic contractile organs like, the pharynx of *C. elegans*, and the vertebrate heart, given the vital role of these organelles in supplying contraction energy (31).

The hypothesis that ROS have a causal role in damaging the pharynx of worms was supported by the observation that antioxidant drugs, known to counteract ROS-induced pharyngeal dysfunction, prevent mitochondrial damage caused by cardiotoxic LC (13).

ROS generated by LC can also trigger important signaling events aimed at limiting and repairing the stress-induced damage. A first line of defence is represented by the activation of chaperones, such as HSP, whose expression can be induced by ROS, metal ions, and misfolded proteins (16). To this end, to gain a better insight into the molecular mechanisms triggered by the oxidative stress caused by cardiotoxic LC, we observed that they activate the expression of HSP-16.2, an αB-crystallin-related protein involved in the metabolism and toxicity of other amyloidogenic proteins (16).

Importantly, we also observed the nuclear translocation of the FOXO/DAF-16 transcription factor, similarly to what happens in response to paraquat administration (9). This transcription factor, member of the evolutionary conserved I/IGF-1-like signaling pathway, regulates a set of stress-responsive genes, including *hsp-16.2* and *sod-3*, and also controls the longevity of *C. elegans*. These studies indicate that metal-mediated ROS generation target mitochondria and activate several intersecting signalling pathways and genes, advancing the understanding of the mechanism underlying LC toxicity.

The effectiveness of using a pharmacological strategy aimed at restoring the metal homeostasis and interrupting the vicious cycle of oxidative stress production caused by metal ions was investigated here. Both 8-hydroxyquinoline compounds proved effective in protecting worms from cardiotoxic LC-induced functional and ultrastructural damage, providing new mechanistic information on amyloid heart disease. Notably, PBT2, acting as metal protein attenuating compound, had beneficial effects on different proteins involved in neurodegenerative diseases such as Alzheimer's and Huntington's diseases (15, 28). In the *C.elegans* model, PBT2 counteracted LC toxicity at a concentration 7000-fold lower than CQ and restored pumping in the presence of LC-induced functional damage, suggesting potential for future translation to clinical use.

The effects displayed by CQ and PBT2 have been shown to derive from multiple mechanisms of action involving both their simple action as (redox silencing) chelator and their ability to act as metal chaperones to promote protective intracellular signaling by transporting metals into the cells (5). We showed that neither compound counteracted H_2O_2-induced pharyngeal dysfunction and mitochondrial ROS generation, indicating that their protective activity against LC toxicity was not ascribable to a direct antioxidant activity (1, 11). Both 8-hydroxyquinoline compounds prevented the induction by LC of pharyngeal expression of HSP-16.2 and SOD-3. In addition, they promoted the nuclear translocation of DAF-16, known to have a prominent influence on disease-related life span changes in *C. elegans* (40, 44), an effect that was not observed when NAC, exerting only an antioxidant activity, was administered.

Although these findings were demonstrated in a simple multicellular organism, the significant evolutionary conservation of basic biological processes between *C. elegans* and humans strongly suggests that metal-induced oxidative stress, already reported to be linked with some neurological disorders (18, 55), is also a key element in cardiac AL. Metal-binding compounds of moderate affinity, which can redistribute biological metals, could be key drugs in an innovative therapeutic strategy designed to target directly the mechanisms of cardiac LC toxicity. In this aspect, PBT2 is particularly promising since it was administered for 26 weeks to Huntington' patients in the absence of side effects (26).

Cardiac involvement in AL is staged using the Mayo Clinic system (14). Patients with advanced cardiac damage (stage III) can be further distinguished in two subgroups, stage IIIa and IIIb, if they present with N-terminal proormone of brain natriuretic peptide below or above 8500 ng/l, respectively. The survival of stage IIIb patients, who represent $\sim$25% of newly diagnosed patients, is a matter of few weeks, using current therapies. Stage IIIb patients represent an unmet need. It has been recently reported, in a case-matched study, that the addition of doxycycline to chemotherapy can significantly reduce the early mortality in patients with stage IIIa, but it is ineffective in patients with stage IIIb (53). The synergic combination of PBT2 with TETRA offers a new therapeutic tool for AL patients with cardiac damage, particularly for stage IIIb patients.

Materials and Methods

Human samples

Urine, bone marrow plasma cells, and endomyocardial biopsies were obtained from patients during routine diagnostic procedures. Acquisition, storage, and use of biological samples for research purposes were approved by the institutional review board. Written informed consent was received from participants before inclusion in the study. The presence of tissue amyloid deposits and amyloid organ involvement were defined according to the International Consensus Panel Criteria (19). LC cardiotoxicity was evaluated on the basis of clinical, echocardiography, and biochemical parameters. Non-amyloidogenic LC from MM patients were used as controls. All LC included in the study were λ isotype, which represents $\sim$75% of amyloidogenic LC.

Human monoclonal LC were isolated from urine (Bence Jones [BJ]) and by production, as recombinant proteins (42, 46). Overall, seven LC were obtained (six BJ and one recombinant) (Supplementary Table S1). Endomyocardial biopsies from three AL patients with advanced cardiac dysfunction and from one subject with primary dilated cardiomyopathy (Supplementary Table S3), used as control for disease and severity of heart dysfunction, were analyzed.

Hydrogen peroxide determination

Cardiotoxic H7-BJ and myeloma MM2-BJ proteins (1 mg/ml, corresponding to 45 μM) in 10 mM phosphate-buffered saline (PBS) (pH 7.4) were incubated in the presence or absence of chelex 100 chelating resin (5 mg/ml, Bio-Rad Laboratories, München, Germany) for 1 h at 4°C with shaking, according to the manufacturer's instructions. PBS and bidistilled water were incubated with chelex in the same conditions. Samples were centrifuged at 8700 $g \times 5$ min at 4°C, supernatants were collected, and the protein content was determined (Bio-Rad Laboratories München, Germany). Different times after incubation, 2 μl of solution was put into a 96-well black plate, diluted 1:100 (vol/vol) with 10 mM PBS, pH 7.4, and the amount of H_2O_2 generated was determined by using the Amplex® Red Hydrogen Peroxide/Peroxidase Assay Kit (Catalog no. A22188; Molecular probes, Life Technologies, Thermo Fisher, Milan, Italy).

To determine the optimal amount of sample for the analysis, from a 20 mM H_2O_2 working solution in 1 × Reaction Buffer (prepared just before use and used within a few hours of preparation), a standard curve from 0 to 10 μM was prepared. In addition, 10 μM H_2O_2 solution in 1 × Reaction Buffer was used as a positive control, and 1 × Reaction Buffer without H_2O_2 was used as a negative control. Additional controls included 10 mM PBS (pH 7.4) and bidistilled water, incubated or not with chelex.

Experiments were done with proteins previously incubated with 50 μM $CuCl_2$, 50 μM $ZnCl_2$, 50 μM $FeCl_2$, 25 μM CQ (dissolved in DMSO at 250 μM; Sigma Aldrich, MO), or 2 nM PBT2 (dissolved in absolute ethanol at 250 μM; Prana Biotechnology Ltd, Parkville, Australia). $CuCl_2$, $ZnCl_2$, $FeCl_2$, CQ, and PBT2 were used as controls. The role of thiols was considered by performing experiments with proteins previously incubated with iodoacetamide (1:10 molar ratio) for 3 h at 20°C (54). Iodoacetamide alone was used as control.

EPR studies

EPR spectroscopy studies were performed as already described (13). Sixty micromolars of cardiotoxic (H7-BJ) and myeloma (MM2-BJ, MM7-BJ) proteins, in 10 mM PBS, pH 7.4, were incubated with or without 30 μM Cu^{2+}. Detection of oxygen radical species by EPR spectroscopy was evaluated by adding the spin-trap 5-(diethoxyphosphoryl)-5-methyl-1-pyrroline-N-oxide (DEPMPO; Enzo Life Sciences, Rome Italy), with a 1000-fold molar excess, as already described (13), on an ESP300 CW-X band spectrometer (Bruker, Milan, Italy). The EPR signal intensity was assessed based on the peak-to-trough height of a reference line in the spectrum.

C. elegans *studies*

Bristol N2 strain, transgenic CL2070, CF1553, and TJ356 were obtained from the *Caenorhabditis elegans* Genetic Center (CGC, University of Minnesota, Minneapolis, MN) and propagated at 20°C on solid nematode growth medium (NGM) seeded with *Escherichia coli* OP50 (CGC) for food. The effect of LC on pharyngeal behavior was evaluated as already described (13). Briefly, worms were incubated with 100 μg/ml LC (100 worms/100 μl) in 10 mM PBS, pH 7.4. Control worms were incubated with 10 mM PBS, pH 7.4 (Vehicle) only. After 2 h of incubation on orbital shaking, worms were transferred onto NGM plates seeded with OP50 *E. coli*.

The pharyngeal pumping rate, measured by counting the number of times the terminal bulb of the pharynx contracted over a 1-min interval, was scored 20 h later. Experiments were also performed by feeding worms for 2 h with 100 μg/ml of LC alone or with 5 mM NAC (Sigma-Aldrich) or 20–50 μM TETRA (Sigma-Aldrich) in 10 mM PBS, pH 7.4; 5 mg/ml chelex in 10 mM PBS, pH 7.4; 10 μM EDTA (Sigma Aldrich) in metal-free water (Sigma Aldrich), 0–25 μM CQ, or 0–25 nM PBT2 dissolved as described above; 50–100 μM copper (from $CuCl_2$) in metal-free water, 50–100 μM zinc (from $ZnCl_2$) in metal-free water, 50–100 μM iron (from $FeCl_2$) in metal-free water. These doses of copper, zinc, and iron, which are well above the physiological levels in humans, are compatible with viability of the worms and may be representative of biologically relevant concentration in *C. elegans* (7, 45). Higher doses of chelex, EDTA, CQ, and PBT2 were proved toxic for nematodes (22, 27).

The effect of 1 mM H_2O_2 for 30 min, alone, or together with 5 mg/ml chelex, 25 μM CQ, or 2 nM PBT2, was also investigated. One mM H_2O_2 and cardiotoxic and myeloma LC (100 μg/ml) were diluted in 50 mM phosphate buffer, pH 7.0, and incubated with 100 U/ml catalase (Sigma Aldrich) for 15 min at room temperature in dark conditions. Nematodes were incubated with these solutions (100 worms/100 μl) for 30 min on orbital shaking in dark conditions and then transferred onto NGM plates seeded with OP50 *E. coli*. The pharyngeal pumping rate was measured 2 h later.

To investigate the combined effect of TETRA and metal-binding compounds, nematodes (100 worms/100 μl) were fed 100 μg/ml H7 alone for 2 h and then treated for 30 min with CQ (25 μM), PBT2 (0.5–2 nM), 20 μM TETRA alone, or together with 0.5–2 nM PBT2. Worms were then transferred onto fresh NGM plates seeded with *E. coli* in the presence of the same drug concentration, and the pharyngeal pumping rate was scored after 20 h. Worms were also exposed to the drugs alone or to vehicle in the same experimental conditions.

For life span experiments, N2 worms (100 worms/100 μl), at L3 larval stage, were fed for 2 h 100 μg/ml of H7 alone or with 25 μM CQ or 2 nM PBT2 (13). Fresh 2 nM PBT2 was daily added to PBT2-treated worms. The number of live worms was determined for each consecutive day until all worms were dead.

Mitochondrial production of ROS

The effect of LC on mitochondrial oxidant burden was evaluated by feeding worms with MitoSOX Red (Molecular Probes, Italy) as already described (13).

Mitochondrial membrane potential

N2 worms were incubated with 100 μg/ml of LC (100 worms/100 μl) in 10 mM PBS (pH 7.4). Negative control worms were incubated with 10 mM PBS (pH 7.4) (vehicle) only and positive control worms were incubated with 10 mM H_2O_2. After a 2-h incubation with orbital shaking, worms were plated on NGM plates seeded with OP50 *E. coli* pretreated for 2 h with 20 μM TMRM (Molecular Probes, Thermo Fisher Scientific). After 24 h, worms were immobilized with 20 mM levamisole and immediately used for microscopic examination with an inverted fluorescent microscope (IX-71 Olympus) equipped with a CCD camera. Images of the pharynges were taken at 40 × magnification with a TRITC filter set (Olympus).

TEM analysis

Worms fed cardiotoxic LC or myeloma alone or with drugs, as described before, were picked, washed in 10 mM PBS, pH 7.4, and fixed with 2% glutaraldehyde in 0.12 M phosphate buffer, pH 7.4. Worms were cut open at the level of second bulb of the pharynx to improve access of the fixative. After postfixation at room temperature overnight, samples were incubated in a solution of 1% OsO_4 and 1.5% ferrocyanide in 0.12 M cacodylate buffer (ferrocyanide-reduced OsO_4) at room temperature for 1 h, then 0.3% thiocarbohydrazide in water for 5 min, and finally 2% OsO_4 in 0.12 M cacodylate buffer for 1 h. *C. elegans* pharynx was then placed into 2% agarose gel and small cubes were cut and dehydrated in graded series of ethanol for 10 min each, cleared in propylene oxide, embedded in epoxy medium (Epon 812 Fluka), and polymerized at 60°C for 72 h.

From each sample, one semithin (1 μm) section was cut with a Leica EM UC6 ultramicrotome and mounted on glass slides for light microscopic inspection. Ultrathin (60–80 nm thick) sections of areas of interest were obtained, counterstained with uranyl acetate and lead citrate, and examined with an Energy Filter TEM (ZEISS LIBRA® 120) equipped with a YAG scintillator slow scan CCD camera.

Specimens of human myocardial tissue were fixed with 2.5% glutaraldehyde in 0.2 M cacodylate buffer, pH 7.3, for 2 h, and postfixed in 1% OsO_4 in the same buffer. They were dehydrated in a graded series of ethyl alcohols and embedded in epoxy resin. Ultrathin sections (60–80 nm thick) were cut, mounted on nickel grids, and stained with 5% uranyl acetate and lead citrate. A minimum of five sections for each patient were observed with a Philips CM12 TEM. Sections were then processed for postembedding immunogold (21). Enzymatic predigestion (0.05% trypsin in 0.05 M Tris buffer with 0.05% $CaCl_2$, 37°C, 15 min) to unmask antigenic epitopes was performed. Sections were rinsed in 0.05 M Tris/HCl buffer, pH 7.3, incubated with either 1:20 normal goat serum or 1% egg albumin for 15 min at room temperature. The sections were incubated overnight at 4°C with a polyclonal anti-λ LC antibody (dilution 1:50; Dako, Agilent Technologies, CA) and then incubated for 1 h at room temperature with protein-A (dilution 1:20) conjugated to 15 nm colloidal gold particles (British Biocell International, United Kingdom). Specificity of immunoreactions was verified using either normal goat serum or egg albumin as primary antibody.

DAF-16 translocation assay and pharyngeal expression of HSP-16 and SOD-3

DAF-16::GFP nuclear translocation was evaluated in TJ356 nematodes. Pharyngeal expression of HSP-16.2::GFP and SOD-3::GFP was determined in CL2070 and CF1553 worms, respectively. Nematodes were fed H7-BJ or MM2-BJ in the absence or presence of CQ, PBT2, TETRA, and NAC as already described. Control worms were incubated with 10 mM PBS, pH 7.4 (vehicle), or drugs alone. After 2–20 h, nematodes were paralyzed by adding 20 mM levamisole, centrifuged at 2000 g for 5 min, and fixed in 4% paraformaldehyde in 10 mM PBS, pH 7.4, for 24 h at 4°C. Organisms were scored as positive for nuclear localization of DAF-16::GFP when green foci were observed throughout the entire body from head to tail and as cytosolic when DAF-16::GFP was diffused. The number of worms with each level of translocation was counted ($n = 100$ worms/condition).

To prove the nuclear localization of activated DAF-16::GFP, nuclear counterstaining was performed with 2′-[4-ethoxyphenyl]-5-[4-methyl-1-piperazinyl]-2,5′-bi-1H-benzimidazole trihydrochloride trihydrate (Hoechst 33342; Thermo Fisher Scientific). Nematodes were fed 100 μg/ml of cardiotoxic H7-BJ LC (100 worms/100 μl) in 10 mM PBS (pH 7.4). Control worms were incubated with 10 mM PBS (pH 7.4) (vehicle) only. After a 2-h incubation with orbital shaking, worms were paralyzed by adding 20 mM levamisole, centrifuged at 2000 g for 3 min, and fixed in 4% paraformaldehyde in 10 mM PBS (pH 7.4) for 2 h at 4°C. Nematodes were centrifuged at 2000 g for 3 min, washed twice with 10 mM PBS (pH 7.4), and resuspended in 0.5 ml of 125 mM Tris-HCl solution (pH 7.4) containing 1% Triton X-100 and 5% β-mercaptoethanol.

After overnight incubation at 4°C, worms were washed with 10 mM PBS (pH 7.4) and incubated at room temperature for 30 min in 0.5 ml of Hoechst (1 mg/ml in 10 mM PBS, pH 7.4). Nuclear translocation of DAF-16 and Hoechst was visualized at 40 × magnification with a GFP and a UV filter, respectively, with an inverted fluorescent microscope (IX-71 Olympus) equipped with a CCD camera. At least 10 worms were photographed per group.

Images for HSP-16.2::GFP and SOD-3::GFP expression in the pharynx of worms were acquired using the same exposure settings. Average pixel intensity values were calculated by sampling images of different animals. Mean pixel intensity for each experimental group was calculated using Cell-F software (Olympus).

Statistical analysis

The data were analyzed using GraphPad Prism 6.0 software (GraphPad Software, CA) by an independent Student's t-test,

one-way and two-way analysis of variance, and Bonferroni's *post hoc* test. The values of IC_{50} and median survival were determined using Prism version 6.0 for Windows (GraphPad Software). A $p < 0.05$ was considered statistically significant.

Acknowledgments

We thank Carmina Natale and Ilaria Craparotta for their help in performing TMRM experiments. This work was supported by Cariplo Foundation Project no. 2015-0591 and no. 2013-0964, Banca Intesa Sanpaolo, Grant 2016, by AIRC (Associazione Italiana per la Ricerca sul Cancro) Special Program Molecular Clinical Oncology 5 per mille (No. 9965), and by the Italian Ministry of Health (GR-2010-2317596). *C. elegans* and OP50 *E. coli* were provided by the GCG, which is funded by NIH Office Research Infrastructure Programs (P40 OD010440).

Author Disclosure Statement

R.A.C. is a paid consultant and a shareholder in Prana Biotechnology Ltd. The other authors have no competing interests.

References

1. Adlard PA, Cherny RA, Finkelstein DI, Gautier E, Robb E, Cortes M, Volitakis I, Liu X, Smith JP, Perez K, Laughton K, Li QX, Charman SA, Nicolazzo JA, Wilkins S, Deleva K, Lynch T, Kok G, Ritchie CW, Tanzi RE, Cappai R, Masters CL, Barnham KJ, and Bush AI. Rapid restoration of cognition in Alzheimer's transgenic mice with 8-hydroxy quinoline analogs is associated with decreased interstitial Abeta. *Neuron* 59: 43–55, 2008.
2. Anbalagan C, Lafayette I, Antoniou-Kourounioti M, Haque M, King J, Johnsen B, Baillie D, Gutierrez C, Martin JA, and de Pomerai D. Transgenic nematodes as biosensors for metal stress in soil pore water samples. *Ecotoxicology* 21: 439–455, 2012.
3. Avery L and Horvitz HR. Pharyngeal pumping continues after laser killing of the pharyngeal nervous system of *C. elegans*. *Neuron* 3: 473–485, 1989.
4. Back P, Braeckman BP, and Matthijssens F. ROS in aging *Caenorhabditis elegans*: damage or signaling? *Oxid Med Cell Longev* 2012: 608478, 2012.
5. Barnham KJ and Bush AI. Biological metals and metal-targeting compounds in major neurodegenerative diseases. *Chem Soc Rev* 43: 6727–6749, 2014.
6. Bhatla N and Horvitz HR. Light and hydrogen peroxide inhibit *C. elegans* Feeding through gustatory receptor orthologs and pharyngeal neurons. *Neuron* 85: 804–818, 2015.
7. Boyd WA, Cole RD, Anderson GL, and Williams PL. The effects of metals and food availability on the behavior of *Caenorhabditis elegans*. *Environ Toxicol Chem* 22: 3049–3055, 2003.
8. Brenner DA, Jain M, Pimentel DR, Wang B, Connors LH, Skinner M, Apstein CS, and Liao R. Human amyloidogenic light chains directly impair cardiomyocyte function through an increase in cellular oxidant stress. *Circ Res* 94: 1008–1010, 2004.
9. Chavez V, Mohri-Shiomi A, Maadani A, Vega LA, and Garsin DA. Oxidative stress enzymes are required for DAF-16-mediated immunity due to generation of reactive oxygen species by *Caenorhabditis elegans*. *Genetics* 176: 1567–1577, 2007.
10. Chin TF and Lach JL. Drug diffusion and bioavailability: tetracycline metallic chelation. *Am J Hosp Pharm* 32: 625–629, 1975.
11. Crouch PJ, Savva MS, Hung LW, Donnelly PS, Mot AI, Parker SJ, Greenough MA, Volitakis I, Adlard PA, Cherny RA, Masters CL, Bush AI, Barnham KJ, and White AR. The Alzheimer's therapeutic PBT2 promotes amyloid-beta degradation and GSK3 phosphorylation via a metal chaperone activity. *J Neurochem* 119: 220–230, 2011.
12. Davis DP, Gallo G, Vogen SM, Dul JL, Sciarretta KL, Kumar A, Raffen R, Stevens FJ, and Argon Y. Both the environment and somatic mutations govern the aggregation pathway of pathogenic immunoglobulin light chain. *J Mol Biol* 313: 1021–1034, 2001.
13. Diomede L, Rognoni P, Lavatelli F, Romeo M, del Favero E, Cantu L, Ghibaudi E, di Fonzo A, Corbelli A, Fiordaliso F, Palladini G, Valentini V, Perfetti V, Salmona M, and Merlini G. A *Caenorhabditis elegans*-based assay recognizes immunoglobulin light chains causing heart amyloidosis. *Blood* 123: 3543–3552, 2014.
14. Dispenzieri A, Gertz MA, Kyle RA, Lacy MQ, Burritt MF, Therneau TM, Greipp PR, Witzig TE, Lust JA, Rajkumar SV, Fonseca R, Zeldenrust SR, McGregor CG, and Jaffe AS. Serum cardiac troponins and N-terminal pro-brain natriuretic peptide: a staging system for primary systemic amyloidosis. *J Clin Oncol* 22: 3751–3757, 2004.
15. Faux NG, Ritchie CW, Gunn A, Rembach A, Tsatsanis A, Bedo J, Harrison J, Lannfelt L, Blennow K, Zetterberg H, Ingelsson M, Masters CL, Tanzi RE, Cummings JL, Herd CM, and Bush AI. PBT2 rapidly improves cognition in Alzheimer's Disease: additional phase II analyses. *J Alzheimers Dis* 20: 509–516, 2010.
16. Fonte V, Kapulkin WJ, Taft A, Fluet A, Friedman D, and Link CD. Interaction of intracellular beta amyloid peptide with chaperone proteins. *Proc Natl Acad Sci U S A* 99: 9439–9444, 2002.
17. Friedly JC, Kent DB, and Davis JA. Simulation of the mobility of metal-EDTA complexes in groundwater: the influence of contaminant metals. *Environ Sci Technol* 36: 355–363, 2002.
18. Gaeta A and Hider RC. The crucial role of metal ions in neurodegeneration: the basis for a promising therapeutic strategy. *Br J Pharmacol* 146: 1041–1059, 2005.
19. Gertz MA, Comenzo R, Falk RH, Fermand JP, Hazenberg BP, Hawkins PN, Merlini G, Moreau P, Ronco P, Sanchorawala V, Sezer O, Solomon A, and Grateau G. Definition of organ involvement and treatment response in immunoglobulin light chain amyloidosis (AL): a consensus opinion from the 10th International Symposium on Amyloid and Amyloidosis, Tours, France, 18–22 April 2004. *Am J Hematol* 79: 319–328, 2005.
20. Giglio MP, Hunter T, Bannister JV, Bannister WH, and Hunter GJ. The manganese superoxide dismutase gene of *Caenorhabditis elegans*. *Biochem Mol Biol Int* 33: 37–40, 1994.
21. Guan J, Mishra S, Qiu Y, Shi J, Trudeau K, Las G, Liesa M, Shirihai OS, Connors LH, Seldin DC, Falk RH, MacRae CA, and Liao R. Lysosomal dysfunction and impaired autophagy underlie the pathogenesis of amyloidogenic light chain-mediated cardiotoxicity. *EMBO Mol Med* 6: 1493–1507, 2014.
22. Harrington JM, Boyd WA, Smith MV, Rice JR, Freedman JH, and Crumbliss AL. Amelioration of metal-induced toxicity in *Caenorhabditis elegans*: utility of chelating

agents in the bioremediation of metals. *Toxicol Sci* 129: 49–56, 2012.
23. Hartwig K, Heidler T, Moch J, Daniel H, and Wenzel U. Feeding a ROS-generator to *Caenorhabditis elegans* leads to increased expression of small heat shock protein HSP-16.2 and hormesis. *Genes Nutr* 4: 59–67, 2009.
24. He Q, Song N, Xu H, Wang R, Xie J, and Jiang H. Alpha-synuclein aggregation is involved in the toxicity induced by ferric iron to SK-N-SH neuroblastoma cells. *J Neural Transm* 118: 397–406, 2011.
25. Hunter T, Bannister WH, and Hunter GJ. Cloning, expression, and characterization of two manganese superoxide dismutases from *Caenorhabditis elegans*. *J Biol Chem* 272: 28652–28659, 1997.
26. Huntington Study Group Reach HDI. Safety, tolerability, and efficacy of PBT2 in Huntington's disease: a phase 2, randomised, double-blind, placebo-controlled trial. *Lancet Neurol* 14: 39–47, 2015.
27. Imbert J, Culotta V, Furst P, Gedamu L, and Hamer D. Regulation of metallothionein gene transcription by metals. *Adv Inorg Biochem* 8: 139–164, 1990.
28. Kenche VB and Barnham KJ. Alzheimer's disease & metals: therapeutic opportunities. *Br J Pharmacol* 163: 211–219, 2011.
29. Lavatelli F, Imperlini E, Orru S, Rognoni P, Sarnataro D, Palladini G, Malpasso G, Soriano ME, Di Fonzo A, Valentini V, Gnecchi M, Perlini S, Salvatore F, and Merlini G. Novel mitochondrial protein interactors of immunoglobulin light chains causing heart amyloidosis. *FASEB J* 29: 4614–4628, 2015.
30. Liao R, Jain M, Teller P, Connors LH, Ngoy S, Skinner M, Falk RH, and Apstein CS. Infusion of light chains from patients with cardiac amyloidosis causes diastolic dysfunction in isolated mouse hearts. *Circulation* 104: 1594–1597, 2001.
31. Mango SE. The *C. elegans* pharynx: a model for organogenesis. *WormBook* 1–26, 2007.
32. Matlack KE, Tardiff DF, Narayan P, Hamamichi S, Caldwell KA, Caldwell GA, and Lindquist S. Clioquinol promotes the degradation of metal-dependent amyloid-beta (Abeta) oligomers to restore endocytosis and ameliorate Abeta toxicity. *Proc Natl Acad Sci U S A* 111: 4013–4018, 2014.
33. Merlini G and Bellotti V. Molecular mechanisms of amyloidosis. *N Engl J Med* 349: 583–596, 2003.
34. Merlini G and Palladini G. Light chain amyloidosis: the heart of the problem. *Haematologica* 98: 1492–1495, 2013.
35. Mishra S, Guan J, Plovie E, Seldin DC, Connors LH, Merlini G, Falk RH, MacRae CA, and Liao R. Human amyloidogenic light chain proteins result in cardiac dysfunction, cell death, and early mortality in zebrafish. *Am J Physiol Heart Circ Physiol* 305: H95–H103, 2013.
36. Moreno-Arriola E, Cardenas-Rodriguez N, Coballase-Urrutia E, Pedraza-Chaverri J, Carmona-Aparicio L, and Ortega-Cuellar D. *Caenorhabditis elegans*: a useful model for studying metabolic disorders in which oxidative stress is a contributing factor. *Oxid Med Cell Longev* 2014: 705253, 2014.
37. Mukhopadhyay A, Oh SW, and Tissenbaum HA. Worming pathways to and from DAF-16/FOXO. *Exp Gerontol* 41: 928–934, 2006.
38. Munday R, Munday CM, and Winterbourn CC. Inhibition of copper-catalyzed cysteine oxidation by nanomolar concentrations of iron salts. *Free Radic Biol Med* 36: 757–764, 2004.
39. Nuvolone M and Merlini G. Systemic amyloidosis: novel therapies and role of biomarkers. *Nephrol Dial Transplant* 2016 [Epub ahead of print] DOI: 10.1093/ndt/gfw305.
40. Ogg S, Paradis S, Gottlieb S, Patterson GI, Lee L, Tissenbaum HA, and Ruvkun G. The Fork head transcription factor DAF-16 transduces insulin-like metabolic and longevity signals in *C. elegans*. *Nature* 389: 994–999, 1997.
41. Ostrerova-Golts N, Petrucelli L, Hardy J, Lee JM, Farer M, and Wolozin B. The A53T alpha-synuclein mutation increases iron-dependent aggregation and toxicity. *J Neurosci* 20: 6048–6054, 2000.
42. Perfetti V, Sassano M, Ubbiali P, Vignarelli MC, Arbustini E, Corti A, and Merlini G. Inverse polymerase chain reaction for cloning complete human immunoglobulin variable regions and leaders conserving the original sequence. *Anal Biochem* 239: 107–109, 1996.
43. Pillai JA. *Neurodegenerative Diseases: Unifying Principles*, edited by Cummings JL. Northants, United Kingdom: Oxford University Press, 2016.
44. Prachayasittikul V, Prachayasittikul S, Ruchirawat S, and Prachayasittikul V. 8-Hydroxyquinolines: a review of their metal chelating properties and medicinal applications. *Drug Des Devel Ther* 7: 1157–1178, 2013.
45. Rebolledo DL, Aldunate R, Kohn R, Neira I, Minniti AN, and Inestrosa NC. Copper reduces Abeta oligomeric species and ameliorates neuromuscular synaptic defects in a *C. elegans* model of inclusion body myositis. *J Neurosci* 31: 10149–10158, 2011.
46. Rognoni P, Lavatelli F, Casarini S, Palladini G, Verga L, Pedrazzoli P, Valentini G, Merlini G, and Perfetti V. A strategy for synthesis of pathogenic human immunoglobulin free light chains in *E. coli*. *PLoS One* 8: e76022, 2013.
47. Shtonda B and Avery L. CCA-1, EGL-19 and EXP-2 currents shape action potentials in the *Caenorhabditis elegans* pharynx. *J Exp Biol* 208: 2177–2190, 2005.
48. Starich TA, Lee RY, Panzarella C, Avery L, and Shaw JE. eat-5 and unc-7 represent a multigene family in *Caenorhabditis elegans* involved in cell-cell coupling. *J Cell Biol* 134: 537–548, 1996.
49. Stoilova T, Colombo L, Forloni G, Tagliavini F, and Salmona M. A new face for old antibiotics: tetracyclines in treatment of amyloidoses. *J Med Chem* 56: 5987–6006, 2013.
50. Valentini S, Cabreiro F, Ackerman D, Alam MM, Kunze MB, Kay CW, and Gems D. Manipulation of in vivo iron levels can alter resistance to oxidative stress without affecting ageing in the nematode *C. elegans*. *Mech Ageing Dev* 133: 282–290, 2012.
51. Wakabayashi T, Nakamura N, Sambongi Y, Wada Y, Oka T, and Futai M. Identification of the copper chaperone, CUC-1, in *Caenorhabditis elegans*: tissue specific coexpression with the copper transporting ATPase, CUA-1. *FEBS Lett* 440: 141–146, 1998.
52. Wechalekar A, Whelan C, Lachmann H, Fontana M, Mahmood S, Gillmore JD, and Hawkins PN. Oral doxycycline improves outcomes of stage III AL amyloidosis—a matched case control study. *Blood* 126: 732–732, 2015.
53. Wechalekar A, Whelan C, Sachchithanantham S, Fontana M, Mahmood S, Foard D, Lane T, Lachmann HJ, Gillmore JD, and Hawkins PN. A matched case control study of doxycycline added to chemotherapy for reducing early mortality in patients with advanced cardiac AL amyloidosis from the alchemy study cohort. *Blood* 124: 3485–3485, 2014.

54. Winterbourn CC and Carrell RW. Oxidation of human haemoglobin by copper. Mechanism and suggested role of the thiol group of residue beta-93. *Biochem J* 165: 141–148, 1977.
55. Wong BX and Duce JA. The iron regulatory capability of the major protein participants in prevalent neurodegenerative disorders. *Front Pharmacol* 5: 81, 2014.
56. Altun ZF and Hall DH. *Handbook of* C. elegans *Anatomy*. In: WormAtlas. www.wormatlas.org/hermaphrodite/pharynx/Phaframeset.html.2016.

Address correspondence to:
Dr. Luisa Diomede
Department of Molecular Biochemistry and Pharmacology
IRCCS-Istituto di Ricerche Farmacologiche ''Mario Negri''
Via G. La Masa 19
Milan 20156
Italy

E-mail: luisa.diomede@marionegri.it

Date of first submission to ARS Central, August 2, 2016; date of final revised submission, January 19, 2017; date of acceptance, January 26, 2017.

Abbreviations Used

AL = immunoglobulin light chain amyloidosis
BJ = Bence Jones
CD = circular dichroism
CGC = *Caenorhabditis elegans* Genetic Center
CQ = 5-chloro-7-iodo-quinolin-8-ol
DEPMPO = 5-(diethoxyphosphoryl)-5-methyl-1-pyrroline-N-oxide
EDTA = ethylenediaminetetraacetic acid
EPR = electron paramagnetic resonance
F = female
FI = fluorescence intensity
FLC = free light chains
FOXO = forkhead transcription factors
GFP = green fluorescent protein
H = heart
Hoechst = 2′-[4-ethoxyphenyl]-5-[4-methyl-1-piperazinyl]-2,5′-bi-1H-benzimidazoletrihydrochloride trihydrate
HSP = heat shock protein
I/IGF-1 = insulin/insulin growth factor-1
LC = immunoglobulin light chains
M = male
MM = multiple myeloma
NAC = *N*-acetyl-cysteine
NGM = nematode growth medium
PBS = phosphate-buffered saline
ROS = reactive oxygen species
SOD = superoxide dismutase
TEM = transmission electron microscopy
TETRA = tetracycline hydrochloride
TMRM = tetramethylrhodamine, methyl ester